Nonflexible Coils in Solution: A Neutron Spin-Echo Investigation of Alkyl-Substituted Polynorbornenes in Tetrahydrofuran

Michael Monkenbusch,*,† Jürgen Allgaier,† Dieter Richter,† Jörg Stellbrink,† Lewis J. Fetters,‡ and Andreas Greiner§

Institut für Festkörperforschung, Forschungszentrum Jülich, D-52425 Jülich, Germany; School of Chemical and Biomolecular Engineering, Cornell University, Ithaca, New York 14853-5021; and FB Chemie und Wissenschaftliches Zentrum für Materialwissenschaften, Philipps-Universität Marburg, D-35032 Marburg, Germany

Received August 17, 2006; Revised Manuscript Received October 25, 2006

ABSTRACT: The dynamics of rigid random polymer coils in dilute solution has been investigated by neutron spin-echo (NSE) spectroscopy. The polymers used were polynorbornenes that consist of chains of the bridged norbornene rings with hexyl (PNBH) or propyl (PNBP) side groups. These polymer molecules have large internal rotation barriers that hinder conformational changes and give each chain a kind of individual shape memory. Thereby the chains exhibit a dynamical stiffness that leads to a significantly retarded relaxation as compared to flexible polyisoprene chains (PI). While the latter perfectly match the prediction of the Zimm model, the polynorbornene spectra display the signature of a dynamical stiffness due to the "frozen" coil conformation of the PNBH or PNBP chains.

1. Introduction

Rigid random coil polymers may be considered as examples of "single chain glasses".[1] Depending on the time scale of observation, these coils should exhibit different mutual interaction due to different equilibration of the conformational degrees of freedom.[2] The addition polymerization[3] of norbornene and its substituted derivatives yield polymers (see Figure 1) that maintain the bridged norbornene ring structure and display high rotational barriers. They also exhibit unusual bulk properties such as good chemical resistance, dense packing in the amorphous state, large refractive indices, high glass transition temperatures (which occasionally exceed the decomposition temperature), and low birefringence. While the optical properties and chemical inertness render these materials as candidates for optical and electronic uses, polynorbornene (PNB) is not melt-processable and possesses pronounced brittleness. These latter two properties and the solubility can be improved by the introduction of side groups R.[4] PNB has been characterized theoretically[5−9] on the molecular scale by a set of rotational potentials having low-energy states separated by large energy barriers.

It would be anticipated that while real systems would exhibit minor angular fluctuations within a single conformer state the transformation from one conformer state to another is an infrequent event. Polymers of this type represent a new family of macromolecules where the chain energy minima of the potential are distributed along the backbone so that nonextended random "frozen" chain or "single chain glass" conformations emerge. This feature must in turn be coupled with a rotational potential characterized by the presence of large activation energies to chain rotation around these barriers. This criterion is met for the PNB family in that a dihedral of 120° exists in combination with rotation barriers of $E_a = 50-100$ kJ/mol. These anticipated barriers may be related to results obtained for another family of molecules with "shape memory based on restricted rotation"[10] with $E_a = 113$ kJ/mol and equilibration times between 1 and 100 days in the temperature range 337−296 K. Analogous estimation of the conformational equilibration rate for the polynorbornenes yields time constants between 0.1 ms and 1 day. Hence, the random coil conformation is immobilized by the high-energy barriers from other conformations at least within the time scale explored by typical experimental methods probing the molecular dynamics. This is expected to have direct consequences on the observable single chain dynamics in solution—a state of play directly accessible by neutron spin-echo spectroscopy.

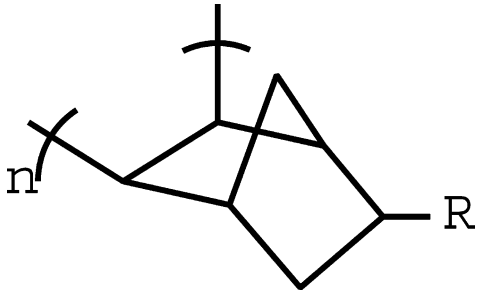

Figure 1. Chemical structure of the hydrocarbon segment of the addition polynorbornene ($n \approx 6000$) used. R denotes a hexane or propane side group.

In this paper we report on the single chain dynamical properties of polynorbornenenes dissolved in tetrahydorfuran (THF) with either propane (poly(5-*n*-propylnorbornene), PNBP) or hexane (poly(5-*n*-hexylnorbornene), PNBH) side groups, R. These samples were prepared by the vinyl type of polymerization with the $[NiBr(NPMe_3)]_4/B(C_6F_5)_3$ catalyst system that leads to the structure shown in Figure 1. For details of synthesis and characterization of the polymers see ref 11. The vinyl-type polymers are soluble in $CHCl_3$, toluene, THF, acetone, and chlorobenzene. Unperturbed chain dimensions in THF solution have been determined[11] in terms of the mean-squared end-to-end distance as $\langle R_e^2 \rangle = 0.311$ Å$^2 \times M$/(g/mol). Estimates of the unperturbed chain dimensions are also available by the application of the Burchard−Stockmayer−Fixman[12,13] approach.

† Forschungszentrum Jülich.
‡ Cornell University.
§ Philipps-Universität Marburg.
* Corresponding author. E-mail: m.monkenbusch@fz-juelich.de.

10.1021/ma0618979 CCC: $33.50
Published on Web 12/08/2006

Table 1. Sample Data

sample	M_w/kg/mol	M_w/M_n	$\langle R^2\rangle_0/M$/[Å^2 mol/g] theta solvent	R_e/Å good solvent	R_e/Å theta solvent	m_b	C_∞
PNB			0.557[a]			47	10.7
PNBP	400	≈2	0.465[b]		431	67	13.3
PNBH	600	≈4	0.311[b]		429	88	11.7
PNBH	350[c]			$300 \times \sqrt{6}$		88	
PI	20	<1.05	0.595	129	109	17	4.7
PI	100	<1.05	0.595	345	244	17	4.7
PI	20	<1.05	*d*	139	116	17	4.7
PI	100	<1.05	*d*	371	259	17	4.7

[a] Cyclohexane: Θ solvent at 34.5 °C. [b] Via Burchard−Stockmayer−Fixman[12,13] approach using THF based intrinsic viscosities. [c] M_w and R_g from static light scattering and SANS. [d] Using relations given in refs 15 and 16 for good solvent cyclohexane and Θ solvent dioxane at 34.7 °C.

2. Experimental Section

2.1. Samples. Polymers from the synthesis described in ref 11 were used for the NSE experiments. Sample data and estimated chain dimensions are shown in Table 1. In order to be able to identify possible effects due to different molecular weights due to the broad distribution of M_w, one of the samples (PNBH) was fractionated. Methanol was added to a 0.1% solution of the polymer at room temperature. The amount of methanol was chosen so that the mixture became clear upon warming to 30 °C. After having cooled the solution again to room temperature overnight in a separating funnel the precipitated high M_w fraction of PNBH was collected and dried. A moderate separation consisting mainly in removal of a short *M* shoulder in the GPC curve could be achieved. The thus-obtained high M_w fraction of PNHB was also analyzed by neutron small-angle scattering (SANS).

Solutions of PNBH, fractionated PNBH (high M_w fraction), and PNBP in deuterated THF were prepared with a weight concentration of 1% and one with 0.5%—in order to identify possible interaction effects—of PNBH (high *M* fraction) and filled into quartz cells (HELLMA) with 4 mm thickness covering a beam cross section of 30 mm × 30 mm (NSE) and 2 or 5 mm thick cells that cover a 10 mm diameter beam (SANS).

The concentration of 0.5% is about the overlap concentration derived from the PNBH data obtained from SANS where $c^* = M/[(4\pi/3)N_A R_g^3] = 0.0049$ g/cm^3 as anticipated from the unperturbed chain dimensions ($R_g = 300$ Å) in Table 1. For comparison, also 1% PI solutions in d-THF were prepared from 20 and 100 kg/mol h-PI synthesized anionically[14] with well-defined molecular weights. The chain dimensions of polyisoprene in good solvent (gs) and theta state are calculated from the following relations: $R_g/\text{Å} = 0.135(M_w/[\text{g/mol}])^{0.61\pm0.01}$ (in cyclohexane; 25 °C) and $R_g/\text{Å} = 0.335(M_w/[\text{g/mol}])^{0.50\pm0.01}$ (in dioxane; 34.7 °C)[15,16] where $R_e \simeq \sqrt{6}R_g$.

2.2. Neutron Scattering. The neutron spin-echo (NSE) and small-angle neutron scattering (SANS) experiments were carried out at the DIDO reactor of the FZ-Jülich.[17] NSE experiments were performed with the NSE-FRJ2 spectrometer using an incoming neutron wavelength band of $\lambda = 8$ Å (fwhm of 10%). NSE measures the intermediate scattering function $S(Q,t)$ (i.e., the Fourier transform of the spectral function $S(Q,\omega)$), which is displayed in normalized form $S(Q,t)/S(Q)$. The wave vector settings and Fourier time range were $Q_0 = 0.05$, 0.08, 0.10, 0.14, and 0.18 Å^{-1} and 0.1 ns < *t* < 22 ns, respectively.

The area detector covers an interval of about [$Q_0 - 0.022$ Å^{-1}, $Q_0 + 0.022$ Å^{-1}] with one setting of the scattering arm to a nominal *Q* value Q_0. The integration over a selected zone can be performed a posteriori and chosen according to the needs of the evaluation (good statistics vs good *Q* resolution). The relaxation curves shown in the following all correspond to integration over the full detector area. Only the display of *Q* dependencies (Figure 7) relies on evaluation of up to five separate detector zones at each setting, Q_0. All experiments were performed at a temperature of 20 ± 0.5 °C. To achieve maximum contrast and minimum incoherent background resulting from protonated material, we used deuterated tetrahydrofuran (d-THF) as solvent. Scattering from corresponding quartz cells containing pure d-THF has been subtracted as background from the NSE and SANS data.

2.2.1. SANS. Small-angle neutron scattering (SANS) experiments were performed on the KWS II instrument at the FRJ2. We used sample-to-detector distances, $D = 20$, 8, and 2 m, and collimation lengths, $L = 20$, 8, and 4 m, using a neutron wavelength $\lambda = 7.3$ Å with a wavelength spread $\delta\lambda/\lambda = 10\%$. This covers a *Q* range of $2 \times 10^{-3} \le Q \le 0.2$ Å^{-1}.

The corresponding scattering length densities

$$\rho_i = \frac{\sum b_z}{v_i} \tag{1}$$

were calculated to be $\rho_{pnh} = 1.371 \times 10^9$ cm^{-2} and $\rho_{d-THF} = 6.346 \times 10^{10}$ cm^{-2}, respectively, assuming the following densities: $d_{pnh} = 0.99$ g/cm^3 and $d_{d-THF} = 0.985$ g/cm^3.

2.3. Light Scattering. Static and dynamic light scattering experiments were performed on an ALV SP-125 (ALV, Germany) compact goniometer using an argon ion laser (Coherent, Innova 90-4), operating with vertically polarized light at $\lambda_0 = 514.5$ nm, $I_0 = 50-800$ mW TEM$_{00}$. Intensity autocorrelation functions $g_2(Q,t)$ were recorded with an ALV 5000 E (fast version, 319 channels) multitau digital correlator covering a time window from 12.5 ns up to several hours. Because of the use of a dual detector system (ALV-SO/SIPD) operating in "pseudo"-cross-correlation mode combined with an optical fiber, even the first channels could be recorded without any distortion from electronic noise. The coherence factor was determined by use of PS latex spheres (PSS, Germany) to be $f_c = 0.93$. All measurements were performed at 20.0 ± 0.1 °C in the angular range 16° ≤ Θ ≤ 154°, yielding a *Q* range from 4.77×10^{-4} to 3.34×10^{-3} Å^{-1}.

Static light scattering data were corrected for background scattering (empty cell, solvent, etc.) and finally scaled to fit to the SANS data, which have been independently normalized to absolute units.

3. Results

3.1. Chain Conformation. The scattering function $S(Q) = S(Q,t=0)$ has been measured with static light scattering and two different neutron instruments, SANS and NSE. Whereas the former extend the range down to *Q* values that correspond to the coil dimension and beyond, the latter (NSE) method enables model free subraction of incoherent background to analyze the local chain statistics without bias.

Figure 2 shows the combined SLS and SANS scattering curves for different concentrations of the fractionated PNBH. The data show the typical form factor of a swollen polymer chain, i.e., an asymptotic power law $I \sim Q^{-5/3}$ in the high *Q* region. The solid lines stem from a simultaneous fit to the Beaucage form factor[18] combined with a virial coefficient; the fit yields $R_g = 300 \pm 1.7$ Å and $A_2 = (11.0 \pm 0.9) \times 10^{-5}$ cm^3 mol g^{-2}. Extrapolation using the Zimm plot in the inset of Figure 2 yields $M_w = 350\,000$ g/mol. The value of $A_2 M_w c[1\%] = 0.36$

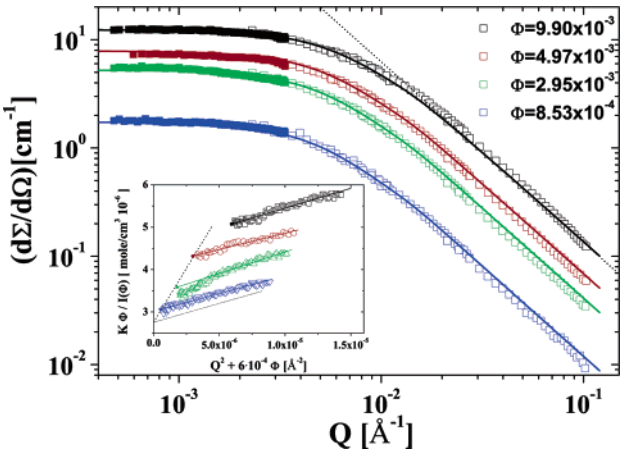

Figure 2. Scattering intensity in absolute units vs scattering vector Q for fractionated PNBH at different concentrations (w:w) obtained by SLS (closed symbols) and SANS (open symbols). Solid line: fit results, see text; dotted line: $I \sim Q^{-5/3}$. The inset shows a Zimm plot for the corresponding data.

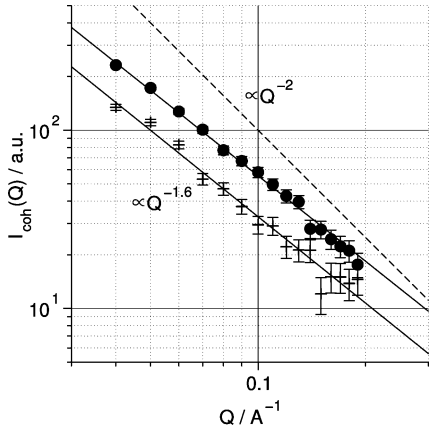

Figure 3. Coherent scattering intensity as measured with the NSE spectrometer in the limited accessible Q range. Solid circles: PNBH; pluses: PI 20K. This is true for both varieties of vinyl-type PNB polymers and also for the PI reference samples; Table 2 lists the fitted values of the exponent ν.

Table 2. Chain Statistics from High Q Asymptote of the Scattering Intensity $I(Q) \propto Q^{-\nu}$

sample	PI 20 kg/mol	PI 100 kg/mol	PNBH	PNBP
ν	1.61	1.61	1.593 ± 0.03	1.641 ± 0.03

indicates that interaction effects are marginal at concentrations of 1% and 0.5%.

The molecular weight, M_w, as determined by SANS is up to a factor of 1.6 lower than the GPC-determined value quoted in Table 1. Here we may accept this discrepancy that may result from the very broad molecular weight distribution because it turns out that none of the NSE results show any indication of a molecular size dependence (see below). The latter is obviously a consequence of the NSE Q range that only allows to probe correlations well inside the polymer coils.

An additonal test of the chain conformation on a local scale was performed with the NSE spectrometer, which was first used in diffraction mode with polarization analysis immediately before the relaxation spectra were measured. Because of the decomposition of coherent and incoherent scattering, which was enabled by the polarization analysis, there is virtually no ambiguity concerning subtraction of incoherent background. The lowest possible Q value of 0.04 Å^{-1} is too large to reach the Guinier regime ($QR_g < 1$); here $QR_g \simeq 0.04 \times 400/\sqrt{6} = 6.5 \gg 1$. Therefore, only the asymptotic high-Q power law $\propto Q^{1/\nu}$

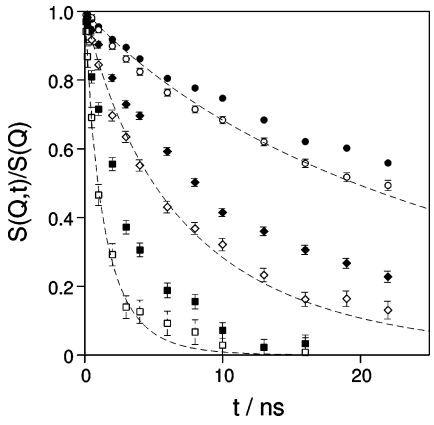

Figure 4. Relaxation spectra of 1% d-THF solution of PI [100 kg/mol] (open symbols) compared to those from a PNBH solution (filled symbols) for $Q_0 = 0.05$ Å^{-1} (circles), 0.08 Å^{-1} (diamonds), and 0.14 Å^{-1} (squares). The dashed lines correspond to the Zimm model prediction (see text).

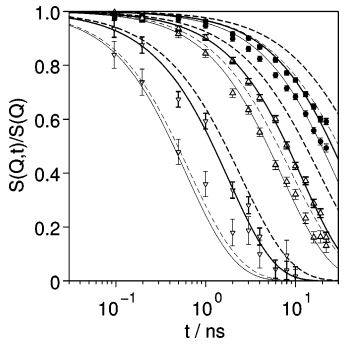

Figure 5. Comparison PI (thin lines) and PNBP (thick lines) for $Q =$ 0.05, 0.08, and 0.18. Dashed lines: center-of-mass diffusion divided out.

can be extracted. Both linear PI solutions yield a value of $1/\nu = 1.61$ close to the value $\nu = 0.61$ measured by DLS[16] and the PNBH and PPNP polynorbornene solutions give $1/\nu = 1.593 \pm 0.03$ and 1.641 ± 0.03, respectively, close to $\nu = 0.6$ as expected for a self-avoiding random coil in a good solvent.[19]

As seen in Figure 3, the value of $1/\nu$ is close to $5/3 = 0.6$ as expected for a self-avoiding random coil in a good solvent. This is true for both varieties of vinyl-type PNB polymers and also for the PI reference samples; Table 2 lists the fitted values of the exponent ν.

3.2. Relaxation Spectra. A comparison of NSE data from the flexible linear reference PI and the PNBH sample both dissolved in d-THF at a concentration of 1% and $T = 20$ °C is shown in Figures 4 and 5. It is obvious that PNBH displays a significantly retarded relaxation compared to that of PI, which virtually displays textbook[19] Zimm behavior (dashed lines) as is discussed below. The retardation effect is much more pronounced and already visible at smaller wavevector, Q, than that observed on a polyisobutylene solution with comparatively small barriers of 13 kJ/mol.[20]

To establish a possible molecular weight dependence and differences between the hexyl- and propyl-type PNB copolymer, we show in Figure 6 the comparison of data from PNBH as synthesized and fractionated to deplete the low molecular weights as well as a juxtaposition of PNBH and PNBP. Within statistical error margins no differences are visible in the relaxation behavior as shown by NSE spectra nor between the fractionated and the nonfractionated PNBH neither between PNBH and PNBP. The same is true for the comparison of the 1% PNBH(fractionated) and 0.5% PNBH(fractionated) solu-

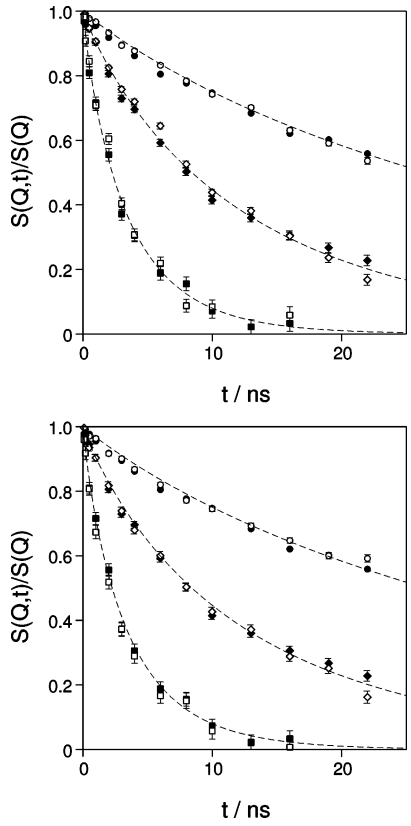

Figure 6. Relaxation spectra as in Figure 4: (a) comparison between PNBH and a high molecular weight fraction of PNBH and (b) between PNBH and PNBP.

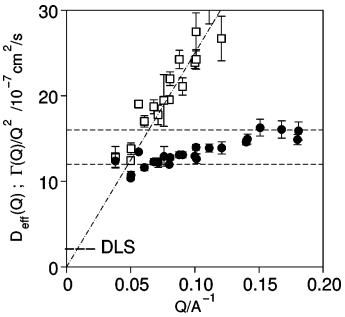

Figure 7. Effective diffusion coefficients for fractionated PNBH (solid circles) and Q^2 scaled rate from $\exp\{-(t\Gamma(Q))^{\beta}\}$ (with $\beta \approx 0.85$) for PI[100 kg/mol] (open squares). DLS indicates the diffusion constant limit $D_{\mathrm{eff}}(Q\rightarrow 0)$ obtained by dynamical light scattering. Within the range of DLS $Q < 0.0334$ Å^{-1} already a slight increase of $D_{\mathrm{eff}}(Q)$ by 10% is encountered. The dashed lines are guides to the eye only.

tions, corroborating that the chosen concentrations in the range of the overlap concentration c^* are sufficiently low. The relaxation curves of PNBH and PNBP can be well fitted with stretched exponentials, $S(Q,t)/S(Q) = \exp[-(t/\tau(Q))^{\beta(Q)}]$, with β values smaller but close to 1 ($\simeq$0.9). This suggests to interpret the data tentatively by a diffusion-type scattering function $S(Q,t)/S(Q) \simeq \exp[-tD_{\mathrm{eff}}(Q)Q^2]$, which yields acceptable fits and an effective diffusion constant as a function of Q, as shown in Figure 7. The $D_{\mathrm{eff}}(Q)$ data show a slight step of about 30% around $Q = 0.12$ Å^{-1}. The extrapolated limiting value $D_{\mathrm{eff}}(Q=0) \simeq (10-12) \times 10^{-7}$ cm^2/s is a factor of up to 5 larger than anticipated for center-of-mass diffusion from the unperturbed chain dimensions. Also, no significant difference is observed between PNBH and PNBP despite the difference in molecular weight. PNBH solution has been investigated by DLS to get an independent value of the center-of-mass diffusion. The experimental DLS data were analyzed independently by the (i) cumulant method[21] or (ii) inverse Laplace transformation using the regularization algorithm of the CONTIN program.[22]

To account for particle interactions in dilute solution, a virial expansion can be made, which describes the concentration dependence of the mutual diffusion coefficient $D_{\mathrm{m}}(\phi)$:

$$D_{\mathrm{m}}(\phi) = D_0(1 + k_{\mathrm{D}}^{\phi}\phi) \tag{2}$$

After extrapolating to infinite dilution, the hydrodynamic radius of the scattering particles can be derived from the Stokes−Einstein relation

$$R_{\mathrm{H}} = \frac{k_{\mathrm{B}}T}{6\pi\eta_0 D_0} \tag{3}$$

with k_{B}, T, and η_0 the Boltzmann constant, the absolute temperature, and the solvent viscosity, respectively.

The thus-obtained dynamical light scattering (DLS) results extrapolated to $Q = 0$ and $\phi = 0$ yield a diffusion coefficient $D_0 = (2.0 \pm 0.2) \times 10^{-7}$ cm^2 s^{-1}, again much lower than the D_{eff} value extrapolated from the NSE data. The corresponding hydrodynamic radius $R_{\mathrm{h}} = 200$ Å for fractionated PNHB; i.e., we obtained a ratio $R_{\mathrm{h}}/R_{\mathrm{g}} \approx 0.66$ as expected for a swollen polymer coil.

In contrast the NSE data of PI (100 kg/mol) exhibit a linear increase of $\Gamma(Q)/Q^2$, i.e., $\Gamma(Q) \propto Q^3$, with $\Gamma(Q) = 1/\tau(Q)$ and $\beta(Q)$ compatible with a value of 0.85. As is show in the next section, the Q^3-dependent rate and $\beta = 0.85$ are the signatures expected from a chain that exhibits normal Zimm dynamics.[23]

3.3. Comparison to the Zimm Model. At intermediate Q values the structure factor for Zimm dynamics can be cast into a master function $S(Q,t)/S(Q) = F(Q^3tkT_{\mathrm{B}}/[6\pi\eta]) = F(\tilde{\Gamma}(Q)t)$, with an universal function $F(x)$:[19,24,25]

$$F(x) = \int_0^{\infty} \exp\left[-u - x^{2/3}\frac{2}{\pi}\int_0^{\infty}\frac{\cos(yux^{-2/3})(1-\exp[-y^{3/2}/\sqrt{2}])}{y^2}\,\mathrm{d}y\right]\mathrm{d}u \tag{4}$$

over the range where most of the decay happens $F(x)$ is close to a stretched exponential $F(x) \simeq \exp[-(x/a)^{\beta}]$ with[23] $a \simeq 1.354$ and $\beta \simeq 0.85$. In that regime $1/\tau(Q) = \Gamma(Q) = \tilde{\Gamma}(Q)/a$. Note that the asymptotic form of $F(x)$ with $\beta = 2/3$ is only valid for larger x, where $F(x) < 10^{-3}$, i.e., beyond the NSE observation range. The Zimm scaling time parameter depends on Q^3 and the solvent viscosity η. The experiments presented here are all performed with deuterated THF at 20 °C as solvent. The tabulated[26] viscosity of deuterated THF at 20 °C is 0.501 mPa·s and 0.557 mPa·s at 15 °C; linear interpolation to 20 °C yields 0.53 mPa·s. To account for the observation that a good description of Zimm dynamics (probably due to the preaveraging approximation of the Oseen tensor) requires a slightly higher effective η (see ref 27), we fix $\eta_{\mathrm{eff}} = 0.55$ mPa·s throughout this paper, which yields a very good description of the PI reference data.

Figure 8 shows scaling plots of the reference samples together with the predictions of the Zimm model. For a finite chain the results of the Zimm model read as follows. The center-of-mass diffusion assuming a Gaussian chain (Θ-solvent) is[19]

$$D_{\mathrm{CM}} = 0.196k_{\mathrm{B}}T/(R_{\mathrm{e}}\eta) \tag{5}$$

for a good solvent the prefactor is 0.203 instead of 0.196. The internal motions including rotational diffusion of the spring-and-bead chain model are described by relaxation modes with

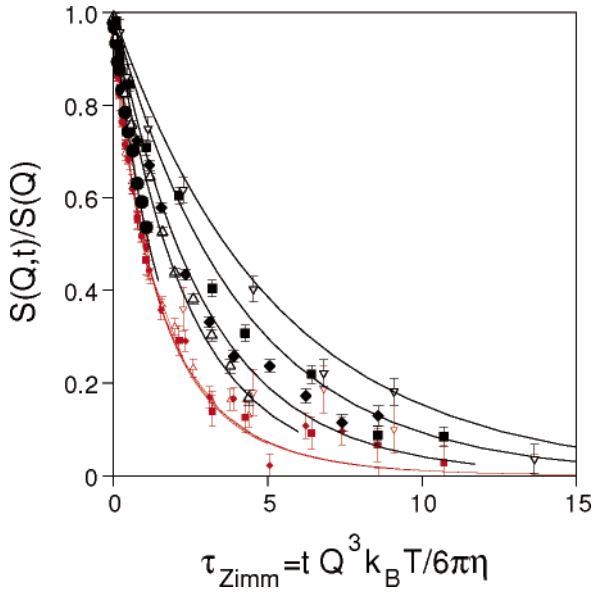

Figure 8. Zimm scaling plot for 100 kg/mol linear PI solution (small symbols) and the high *M* fraction of hexyl-PNB (large black symbols), $Q_0/\text{Å}^{-1} = 0.05$ (solid circle), 0.08 (triangle up), 0.10 (solid diamond), 0.14 (solid square), and 0.18 (triangle down). The solid lines correspond to fits to the discrete Zimm model.

mode number p and characteristic times τ_p:

$$\tau_p = \frac{\eta R_e^{\,3}}{\sqrt{3\pi} k_B T} p^{-3\nu} \tag{6}$$

with the modifications suggested in ref 19 for good solvent with $\nu = 0.6$—inserting $\nu = 1/2$ yields the Gaussian chain expression—$S(Q,t)$ is computed:

$$B(m,n,t) = |n-m|^{2\nu} l^2 + \frac{4R_e^{\,2}}{\pi^2} \sum_{p=1}^{p_{max}} \frac{1}{p^{2\nu+1}} \cos\left(\frac{\pi p n}{N}\right) \cos\left(\frac{\pi p m}{N}\right)(1 - e^{-1/\tau_p})$$

$$S(Q,t) = \sum_{m,n}^{N} e^{-Q^2 D_{CM} t - (Q^2/6) B(m,n,t)} \tag{7}$$

where $l^2 = (R_e^2/N^{2\nu})$. The physical relevant parameters that enter eq 7 are the chain dimension R_e and the viscosity η. Once N is chosen large enough the resulting $S(Q,t)/S(Q)$ is independent of N and the resulting effective "bond length" l_{eff}. Equation 7 perfectly describes the NSE results for the reference PI solutions without further adjustments.

The thin lines in Figure 8 correspond to the computation of $S(Q,t)/S(Q)$ ($R_e = 346$ Å for PI with 100 kg/mol).

In contrast to those from PI, the data from PNBH and PNBP solutions do *not* scale according to the Zimm prediction and exhibit a significantly retarded relaxation compared to the reference solutions. The observed relaxation is still faster by a factor 2−3 than the expected center-of-mass diffusion. Even if we consider the polynorbornenes as rigid random coils besides the center-of-mass diffusion, there should be an additional contribution to the relaxation due to rotational diffusion. Within the Zimm model the rotational diffusion is described by the first mode ($p = 1$). The corresponding scattering function can be computed using eq 7 but keeping only the first term of the *p*-summation. However, with the given coil dimensions it turns out that this procedure is not sufficient to account for the

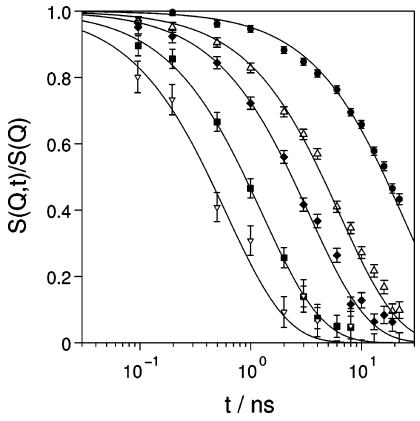

Figure 9. NSE data (symbols $Q/\text{Å}^{-1} = 0.05$: solid circles; 0.08: triangles up; 0.1: solid diamonds; 0.14: solid squares; 0.18: triangles down) from a 1% solution 20 kg/mol PI in d-THF at 200 °C compared to the prediction of the Zimm model, eq 7.

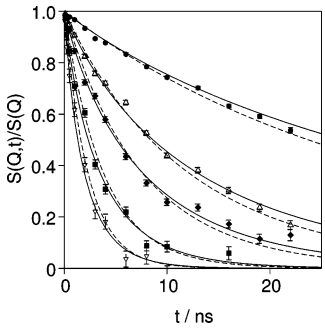

Figure 10. Data from PNBH (high *M* fraction) compared to the Zimm model variants; solid line with stiffness coefficient $\alpha = 0.077$, dashed line with explicit mode limitation to $p_{max} = 11$.

observed relaxation rates. Now, allowing some further internal motions by including not only the first mode but a few more modes up to a cutoff p_{max} yields a very good representation of the PNBH and PNBP data, as is illustrated by the dashed lines in Figure 10 for the high *M* fraction of PNBH with $p_{max} \simeq 11$ (if the fit is performed with $R_e = 450$ Å, for the scaling properties of p_{max} and R_e see the discussion below). Since the reason for the suppression of higher modes is thought to be chain stiffness, a description of the effect may also be achieved by adding a fourth-order term to the effect of the entropic spring constant which contributes proportional to p^2 in Fourier representation.[28,29] The stiffness effect is then semiempirically represented by replacing p^2 with $(p^2 + \alpha p^4)$ in the corresponding expressions. In eq 7 this affects the relaxation mode spectrum spectrum $\tau_p \propto 1/(p^{3\nu} + \alpha p^{4-\nu})$ and the prefactor of the cosine product in the *p*-summation $1/(p^{2\nu+1} + \alpha p^4)$. A fit of this expression with unlimited *p*-summation yields $\alpha = 0.077$ and $S(Q,t)/S(Q)$ as displayed by the solid lines in Figure 10. Limitation of modes or introduction of a stiffness parameter α yields similar relaxation curves that are both compatible with the data. In both cases higher modes are suppressed: in the first case explicitly and in the latter case by the prefactor $1/(p^{2\nu+1} + \alpha p^4)$ where the p^4 term reduces the importance of higher modes. Figure 11 displays a comparison of fits of α to match NSE data of PNBP and PNBH. There is an implict correlation of the resulting value for α with the entered coil dimension R_e. In parallel also the cutoff p_{max} which is necessary to describe the data in the alternative approach decreases when R_e is reduced. Systematic variation of the input value for R_e to the fit procedure reveals the dependence of α and p_{max}, respectively, on R_e, as shown in Figure 12. In particular, the maximum mode number allows a straightforward determination of the size of

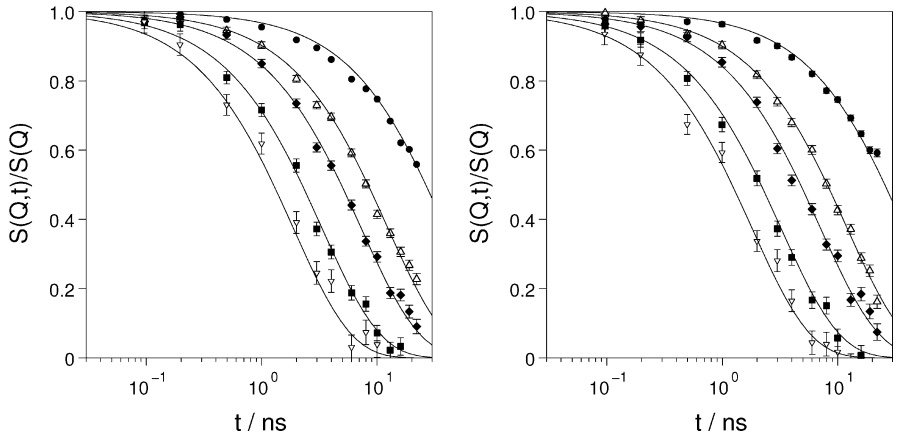

Figure 11. Comparison of NSE data from PNBH and PNBP with the stiffness modified Zimm model with (R_e = 353 Å, α = 0.16) and (R_e = 430 Å, α = 0.08), respectively.

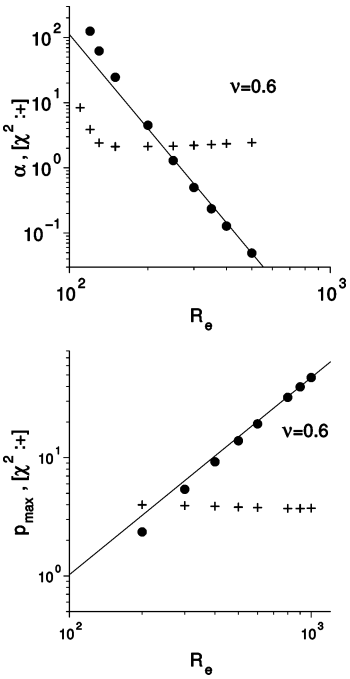

Figure 12. Correlation of the fitted value for the stiffness coefficient α, the maximum mode number p_{max}, and the assumed (fixed) chain extension R_e. The line corresponds to $\alpha \propto (R_e^{2\nu})^{-4}$ to $p_{max} \propto R_e^{1/\nu}$. Plus signs indicate the χ^2 values of the fits.

the moving regions in the norbornene coils. Chain statistics yields $R_e = N^{\nu} l_{eff}$ if N segments of effective length l_{eff} are assumed. Mapped onto the linear chain coordinate n the limiting mode p_{max} leads to displacements $X_{p_{max}}(n) \propto \cos(\pi p_{max} n/N)$; i.e., the typical extension in terms of segments is $n = N/p_{max}$, which leads to an end-to-end distance of the coherently moving subcoil $r_e = n^{\nu} l_{eff}$, i.e., $r_e = R_e p^{-\nu}$. Inserting typical numbers (R_e = 450 Å) × $11^{-0.6}$ = 107 Å within which the subcoils behave virtually rigid. Because of the scaling properties $p \propto R_e^{1/\nu}$ as displayed in Figure 12, this result is virtually independent of the exact choice of R_e during this procedure if it is only large enough. This also explains the independence of the experimental results on fractionation and on the exact value and distribution of molecular weight.

4. Conclusion

The results of the NSE experiments strongly support the hypothesis that the polynorbornenes form nearly frozen coils in solution. The power law type scattering intensity $S(Q,t=0) \propto Q^{-1/(\nu \simeq 0.6)}$ indicates that during or after synthesis the polymer is able to reach the equilibrium conformation of a flexible chain in a good solvent. Both conclusions are consistent with the estimated conformation equilibration time scale of 0.1 ms to 1 day given above. Strictly speaking, the present NSE experiment only allows to restrict the equilibration time scale to any value above a few 100 ns. However, the dynamic response $S(Q,t)$ significantly deviates from a flexible polymer like PI, which has been measured to serve as reference. While the latter exhibits textbook Zimm dynamics and scaling, the relaxation from polynorbornenes violates the scaling and lags behind the pure Zimm relaxation. Its Q dependence rather resembles diffusion with a weak Q dependence of the effective diffusion constant. Still the value of the effective diffusion constant at low Q is 2−3 times larger than that expected for center-of-mass diffusion of a rigid coil. Inclusion of rotational diffusion corresponds to the effect of the first Zimm mode, which turns out to be not enough. To describe the observed relaxation, inclusion of the p_{max} first Zimm modes (11 for R_e = 450 Å) is necessary. The corresponding model describes all data with only one free parameter, the mode cutoff p_{max}. Together with the assumed chain length—as expressed by R_e—this parameter leads to the invariant physical value $r_e = R_e p_{max}^{-\nu}$ of the end-to-end radius of the virtually stiff chain sections. Alternatively, a local stiffness parameter α which adds a αp^4 term to the chain deformation (bending) energy may serve as single parameter to yield equally good (or even slightly better) fits to the experimental data. The mode cutoff may be interpreted in terms of virtually rigid subcoils with all internal modes suppressed, which have a size of $r_e \simeq 107$ Å.

These results may be explained by the assumption that the actual conformation corresponds to a highly degenerated potential minimum that is separated from equivalent conformations by reasonably high-energy barriers such that at least within the observation time of the NSE experiment (i.e., ≃100 ns) no rearrangement is possible. But during macroscopic time interval (e.g., the time between sample prepration and experiment) an equilibrium coil conformation can be attained. An analogous scenario of a dynamically stiff chain that resembles a "stiff bent wire" model has been discussed to explain observations pertaining high-frequency oscillatory birefringence of polymer solutions.[30,31] To arrive at a model consistent with the existence of normal long-wavelength Zimm modes ($p < p_{max}$), it must be assumed that the entropic spring effectively acts only over larger (topological) distances.

The bending stiffness is important at lower distance, i.e., higher modes, and overseeds and thereby supresses any entropic spring effects there. This explains the obvious validity of the

Zimm modes with low mode number and the lack of higher modes in a natural way and corroborates the expectation that polynorbornenes in solution exhibit some properties of a frozen random coil.

Acknowledgment. We thank D. Y. Yoon for drawing our attention to the peculiar properties of polynorbornenes which lead to the presented experiment.

References and Notes

(1) DeGennes, P. G. *Scaling Concepts in Polymer Physics;* Cornell University Press: Ithaca, NY, 1979.
(2) Raos, G.; Allegra, G. *Macromolecules* **1996**, *29*, 6663−6670.
(3) Janiak, C.; Lassahn, P. *Macromol. Rapid Commun.* **2001**, *22*, 479−492.
(4) Grove, N.; Kohl, P.; Allen, S.; Jayaraman, S.; Shick, R. *J. Polym. Sci., Part B: Polym. Phys.* **1999**, *37*, 3003−3010.
(5) Haselwander, T.; Heitz, W.; Krugel, S.; Wendorff, J. *Macromolecules* **1997**, *30*, 5345−5351.
(6) Haselwander, T.; Heitz, W.; Krugel, S.; Wendorff, J. *Macromol. Chem. Phys.* **1996**, *197*, 3435−3453.
(7) Heitz, W.; Krugel, S.; Madan, R.; Wendorff, J. *Macromol. Chem. Phys.* **1999**, *200*, 338−347.
(8) Ahmed, S.; Bidstrup, S.; Kohl, P.; Ludovice, P. *J. Phys. Chem. B* **1998**, *102*, 9783−9790.
(9) Krugel, S.; Raubacher, F.; Wendorff, J. *Macromol. Chem. Phys.* **1998**, *199*, 757−762.
(10) Choi, D.-S.; Chong, Y.; Whitehead, D.; Shimizu, K. *Org. Lett.* **2001**, *3*, 3757−3760.
(11) Müller, K.; Kreiling, S.; Dehnicke, K.; Allgaier, J.; Richter, D.; Fetters, L.; Jung, Y.; Yoon, D.; Greiner, A. *Macromol. Chem. Phys.* **2006**, *207*, 193−200.
(12) Burchard, W. *Makromol. Chem.* **1961**, *50*, 20−36.
(13) Stockmayer, W.; Fixman, M. *J. Polym. Sci., Part C* **1963**, *1*, 137.
(14) Morton, M.; Fetters, L. J. *J. Rubber Chem. Technol.* **1975**, *48*, 359.
(15) Tsunashima, Y.; Hirata, M.; Nemoto, N.; Kajiwara, K.; Kurata, M. *Macromolecules* **1987**, *20*, 2862−2866.
(16) Tsunashima, Y.; Hirata, M.; Nemoto, N.; Kurata, M. *Macromolecules* **1987**, *20*, 1992−1999.
(17) Since the end of 2005 the FRJ2 instruments are moving to the new research reactor FRMII in Munich where they will resume operation end of 2006 with a considerably enhanced intensity and resolution.
(18) Beaucage, G. *J. Appl. Crystallogr.* **1995**, *28*, 717.
(19) Doi, M.; Edwards, S. *The Theory of Polymer Dynamics*; Vol. 73 of *International Series of Monographs on Physics*; Oxford University Press: Oxford, 1994.
(20) Arbe, A.; Monkenbusch, M.; Stellbrink, J.; Richter, D.; Farago, B.; Almdal, K.; Faust, R. *Macromolecules* **2001**, *34*, 1281−1290.
(21) Koppel, D. E. *J. Chem. Phys.* **1972**, *57*, 4814.
(22) Provencher, S. W. *Comput. Phys. Commun.* **1982**, *27*, 213.
(23) Richter, D.; Monkenbusch, M.; Arbe, A.; Colmenero, J. *Neutron Spin Echo in Polymer Systems*; Adv. Polym. Sci. 174; Springer: Berlin, 2005.
(24) Zimm, B. *J. Chem. Phys.* **1956**, *24*, 269.
(25) Dubois-Violette, E.; DeGennes, P. G. *Physics* **1967**, *3*, 181.
(26) Wohlfarth, C.; Wohlfarth, B. *Landolt Boernstein New Series IV/18B;* Springer: Berlin, 2002.
(27) Ewen, B.; Richter, D. *Adv. Polym. Sci.* **1997**, *134*, 1−129.
(28) Richter, D.; Monkenbusch, M.; Allgeier, J.; Arbe, A.; Colmenero, J.; Farago, B.; Bae, Y. C.; Faust, R. *J. Chem. Phys.* **1999**, *111*, 6107−6120.
(29) Harnau, L.; Winkler, R.; Reineker, P. *J. Chem. Phys.* **1997**, *106*, 2469−2476.
(30) Larson, R. *Macromolecules* **2004**, *37*, 5110−5114.
(31) Inoue, T. *Macromolecules* **2006**, *39*, 4615−4618.

MA0618979